Available online at www.sciencedirect.com
ScienceDirect
Advances in Space Research 38 (2006) 979–985
ADVANCES IN SPACE RESEARCH (a COSPAR publication)
www.elsevier.com/locate/asr

Spectral and temporal properties of narrowband dm-spikes and broadband pulses in the August 5, 2003 flare

R.A. Sych [a,b,*], H.S. Sawant [a], M. Karlický [c], H. Mészárosová [c]

[a] INPE – National Institute of Space Reasearch, São José dos Campos, SP, Brazil
[b] ISTP – Institute of Solar Terrestrial Physics, Irkutsk, Russia
[c] Ondřejov Observatory, Ondřejov, Czech Republic

Received 13 October 2004; received in revised form 16 December 2005; accepted 30 December 2005

Abstract

On August 5, 2003 the Ondřejov radiospectrograph and the Brazilian Solar Spectrograph recorded simultaneously the narrowband dm-spikes superimposed on broadband pulses in the frequency ranges of 0.8–4.5 and 1.75–2.25 GHz, respectively. Using a new method of wavelet filtering broadband sub-second pulses with a frequency width of 0.48 GHz and narrowband millisecond spikes with a frequency width 0.13 GHz were recognized and analysed in detail. Filtered radio spectra showed that the spikes were clustered in stripes at different frequencies. These stripes drifted and their frequency ratios changed during short time intervals. Periods of the narrowband spikes and their stripes were ~0.4 s and 4, 8–10, and 16 s, respectively. The main period of the broadband pulses was ~4 s. Values of significant periods of the narrowband spikes coincided with those of the broadband pulses. We found significant peak-to-peak correlations with zero time lags among stripes of the narrowband spikes on different frequencies. The characteristics of the narrowband dm-spikes and broadband pulses indicate that mutually linked emission processes generate both fine structures.

Keywords: Solar flares; Radio spikes; Wavelet filtration; Frequency width

1. Introduction

Narrowband millisecond spikes have been observed for more than two decades over a wide frequency range 0.2–3.0 GHz. The main characteristics of spike are: duration 3–100 ms, a circular polarization up to 100%, a brightness temperature in the range of 10^{10}–10^{15} K, and a narrow width close to the frequency resolution of radio spectrographs (Benz, 1986; Benz and Güdel, 1987). They form clusters (stripes) which are often observed in separated frequency bands having fixed frequency ratios, e.g., 2:3, 3:4, 2:3:4, and 3:4:5 (Güdel, 1990 and references therein). Using the methods of nonlinear dynamics Isliker (1992) analyzed a group of the narrowband dm-spikes and he found that their fractal dimension is very high (almost ∞). Nowadays, the most widely used methods for their analysis are the correlation and Fourier methods (Costa et al., 1990; Marsch and Tu, 1993). However, in the last decade new approaches appeared and they also have been used for the analysis of dm-spikes. These new methods are: multifractal methods (Milovanov and Zelenyi, 1993), singular spectrum analysis (Golyandina et al., 2001), methods based on empirical and complex orthogonal functions (Huang et al., 1999), and multiscale wavelet analysis (Meyer and Roques, 1993).

In the present paper, we analyze the August 5, 2003 event with a unique series of broadband pulses and narrowband dm-spikes. We have used the new techniques mentioned above. We also developed and used new software to carry out wavelet analysis of spikes in stripes, construct filtered dynamic radio spectra, and to compute correlation and cross-correlation of the frequency bands, and Global Wavelet Spectra (GWS) of each frequency band.

* Corresponding author.
E-mail address: sych@iszf.irk.ru (R.A. Sych).

0273-1177/$30
doi:10.1016/j.asr.2005.12.017

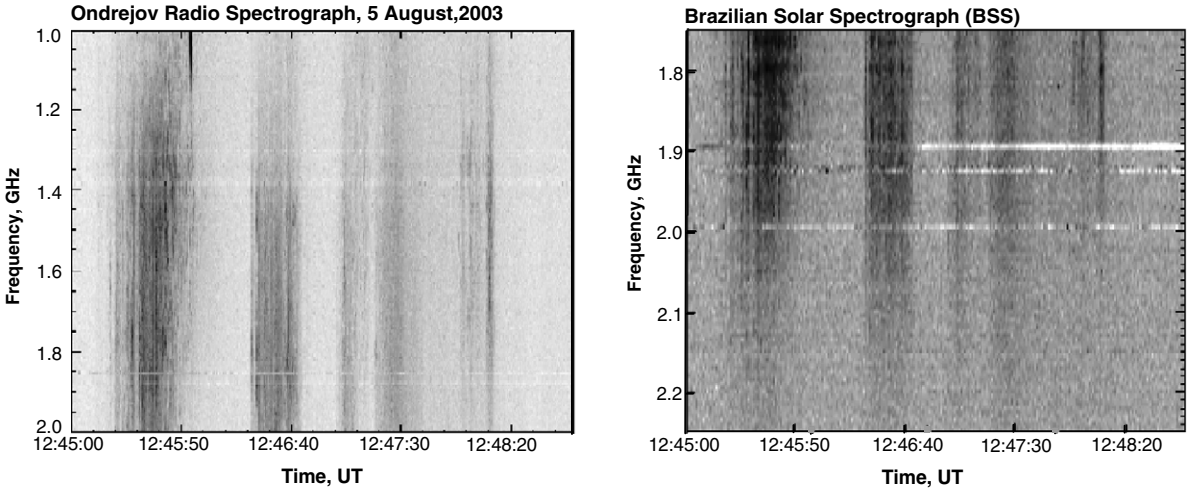

Fig. 1. Global overview of the August 5, 2003 burst in decimetric range. (Left) Dynamic spectrum observed by the Ondřejov radio spectrograph in the 1.0–2.0 GHz frequency range. (Right) Brazilian Solar Spectrograph (BSS) dynamic spectrum (1.75–2.25 GHz). Both instruments have the same time resolution of 100 ms.

2. Observations

On August 5, 2003 at 12:43–16:00 UT, an X-ray M1.7 (GOES 12, 1-8 A) flare occurred in active region AR 0424 located at S18 E39. This active region was a typical bipolar group of spots, with Zurich class Eki and Beta-Gamma magnetic configuration. GOES 12 recorded an impulsive phase with fast rise and fall time and a gradual phase during the time intervals of 12:43–12:55 UT and 12:55–16:00 UT, respectively. Radio observations were made by the Brazilian Solar Radio Spectrograph operating in the frequency range of 1.75–2.25 GHz and the solar radio spectrograph at the Ondřejov Observatory operating in the frequency range of 0.8–2.0 GHz with time resolution of 100 ms.

Fig. 1 shows six groups of decimetric pulses and the narrowband spikes observed during the period of 12:45:00–12:48:50 UT. Details of their timings are listed in Table 1 (see also Fig. 5). The first group observed at 12:45:25–12:45:50 UT, in the frequency range of 1.00–2.25 GHz consists of a series of broadband (0.5 GHz) pulses centered around 1.6 GHz and having global negative drift. Superposed on them, at frequencies ~1.1, 1.3, 1.5 and 1.8 GHz, are stripes of spikes with positive and negative frequency drifts. The most intense dm-spikes with the frequency width of about 0.13 GHz are observed at 1.47 and 1.85 GHz. In the second selected group of pulses, recorded during the time interval of 12:46:25–12:46:44 UT, broadband pulses and stripes of spikes are observed at almost the same frequencies. The other four groups selected show similar behaviour.

Table 1

Time (UT)		Significant frequency width (GHz)			
1st group	12:45:25–12:45:50	0.08	0.14	0.40	0.56
2nd group	12:46:25–12:46:44	0.09	0.16	–	0.56
3rd group	12:47:04–12:47:17	–	0.15	–	0.67
4th group	12:47:20–12:47:35	–	0.15	–	0.67
5th group	12:47:57–12:48:08	0.07	0.18	0.43	0.57
6th group	12:48:08–12:48:13	0.07	0.18	0.40	0.57
Whole burst	12:45:25–12:48:13	0.08	0.15	0.43	0.56

3. Method of analysis

3.1. Dynamic wavelet filtration

To obtain information about spectral properties and distributions of fine structures in the dynamic radio spectrum we have developed a method allowing us to estimate their frequency width by using dynamic wavelet filtration. The basis of the method is the selection of frequency widths of radio features using the Wavelet transform as a frequency filter and the construction of new radio spectra showing filtered features only.

The continuous Wavelet transform is performed through a convolution of the studied function $f(t)$ with a wavelet function $\psi_{a,b}$ (Astaf'eva, 1996) having two parameters. Furthermore, any wavelet function $\psi_{a,b}$ of a given family is obtained from the "parent" function ψ through an extension-contraction and shift

$$\psi_{ab}(t) = |a|^{-1/2}\psi\left(\frac{t-b}{a}\right), \tag{1}$$

where the parameter a is the wavelet width, and b is the shift parameter. Thus, all Wavelet functions of a given family are self-similar and have a constant number of oscillations.

The integral Wavelet transform $(W_\psi f)(a,b)$ of the function $f(t)$ is

$$(W_\psi f)(a,b) = |a|^{-1/2}\int_{-\infty}^{+\infty} f(t)\overline{\psi\left(\frac{t-b}{a}\right)}\,\mathrm{d}t = \int_{-\infty}^{+\infty} f(t)\overline{\psi_{ab}}(t)\,\mathrm{d}t. \tag{2}$$

Moreover, the function ψ must satisfy the condition

$$C_\Psi = 2\pi \int_{-\infty}^{\infty} \frac{|\hat{\psi}(\omega)|^2}{|\omega|}\, d\omega < \infty, \quad (3)$$

where $\hat{\psi}(\omega)$ is the Fourier transform of the function $\psi(t)$.

Because the Wavelet transform, henceforward refereed as WT, is a broadband filter with a known response function (base wavelet), it is possible to reconstruct the signal using its inverse transform in the form of an inverse filter (Donoho and Johnstone, 1994). This is suitable for the orthogonal WT that has an orthogonal basis. Nevertheless, for the continuous Wavelet transform this is complicated because of the redundancy in space and time. In this case, the series represents the sum of the real part of WT of all scales. With the basic parameters (a, b) there exists a formula for the inverse WT

$$f(t) = C_\psi^{-1} \int\int (W_\psi f)(a,b)\psi_{ab}(t) \frac{da\, db}{a^2}, \quad (4)$$

where C_Ψ represents the coefficients of the Fourier transform obtained from Eq. (3).

In contrast to the Fourier transform, the WT retains the locality of the representation of the signal, which makes it possible to reconstruct the signal locally (Torrence and Compo, 1998). In addition, there is a possibility to reconstruct a part of the signal or select the contribution of a certain scale. The local behaviour of the signal and its wavelet-coefficients are related. Hence, to obtain a partial reconstruction of the signal, it is necessary to consider the coefficients referring only to the corresponding sub-region of the wavelet space. Since $(W_\psi f)(a,b)$ contains information about the analyzing wavelet and the input signal, the selection of the analyzing wavelet determines which information should be extracted from the signal. Each wavelet has characteristic properties in time and frequency space. Therefore, using different wavelets it is possible to extract details of the properties of the analyzed signal. In the present case, we have used a complex basis using the Morlet's wavelet (Grossman and Morlet, 1984), which is well localized in the scale, space and frequency planes. In real space, the Morlet's wavelet function consists of a complex exponential modulated by a Gaussian envelope

$$\Psi_0 = \pi^{-1/4} s^{-1/2} \exp[ikt/s] \exp[-(t/s)^2/2], \quad (5)$$

where s is the wavelet scale, k is a non-dimensional parameter, and t is the position.

The application of the direct and inverse Wavelet transforms to dynamic radio spectra has enabled us to select frequency widths of fine structures in radio spectra (spikes, background radio emission) and to investigate their time evolution. This is achieved as follows:

(i) The Global Wavelet Spectrum with 95% confidence level is constructed from the time profile at each frequency in the radio spectrum and hence a histogram of frequency widths can be obtained.
(ii) Thus, we know what frequency widths prevail during the investigated time interval. With these widths, the filtration of the radio spectrum is carried out using the Wavelet transform. At a given time of the radio spectrum, we calculate the frequency profile in narrow spectral band by using different frequency widths. Repeating this process in time, for all groups of pulses, we obtain a filtered radio spectrum. The proposed method enables us to select typical fine structures in the radio spectra of various frequency scales, e.g., from narrowband spikes up to broadband pulses and to trace their time evolution, e.g., their drifts rates, cross correlation, etc.

3.2. Test of the method

To test this method and to obtain information about possible artifacts and restrictions, we simulated a radio spectrum of known frequency characteristics. The model spectrum of the burst with duration of 6 s was constructed in the frequency range (1.0–2.0) GHz (Fig. 2a), including a set of four bands of multiple harmonics with the frequency width 0.13 GHz and period of 0.2 s and a broadband background with the frequency width 0.50 GHz, period of 3.0 s

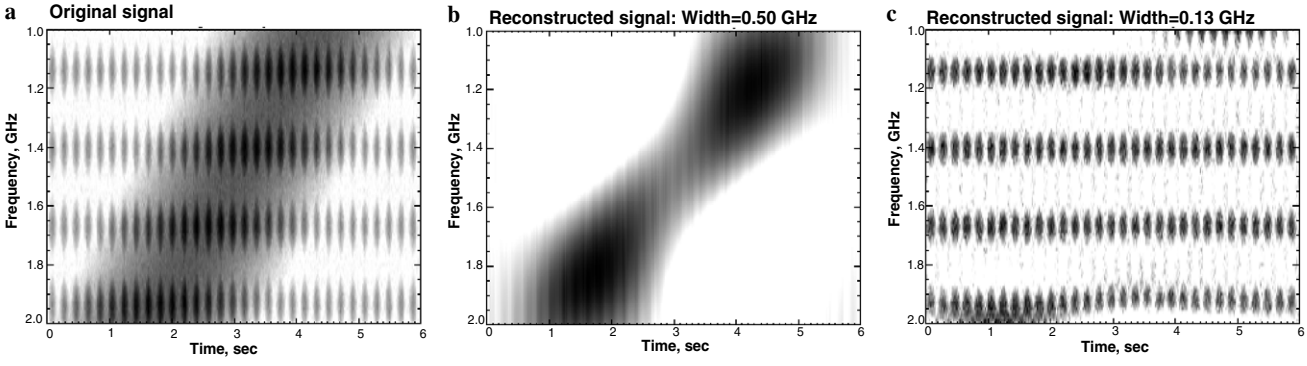

Fig. 2. Test of the method used: (a) the dynamic radio spectrum of the model burst composed of the broadband drifting component with the frequency width 0.50 GHz and four narrowband components with the frequency width 0.13 GHz, modulated in time. (b) The dynamic spectrum of the component with the frequency width 0.50 GHz reconstructed from the dynamic spectrum shown in (a). (c) The same as (b), but for the narrowband components with the frequency width 0.13 GHz.

and frequency drift 0.28 GHz s^{-1}. Then, analyzing this artificial radio spectrum by the method described above we obtained filtered dynamic radio spectra (Figs. 2b and c).

This analysis has shown that the proposed method allows us to distinguish the broadband (0.50 GHz) and narrowband (0.13 GHz) components with details such as simulated frequency bands and simulated drifts. The behaviour of the frequency widths of the spectral details for different temporal periods shows a squeeze of the narrowband component but the magnitude of this squeeze is insignificant (0.01%) and it can be neglected. With an increase of the period of the oscillating component near the period of the background burst, the value of the squeeze increases. This effect is connected with a power increase of the broadband component in the wavelet spectrum. Furthermore, we found deviations of the intensity of the broadband (background) burst (Fig. 2b) comparing with the simulated burst (Fig. 2a). This is due to boundary effects in the wavelet spectrum, especially in cases where the period of the signal is longer than its duration.

3.3. Data analysis

In order to obtain frequency widths of spectral features in six time intervals (Table 1) of the August 05, 2003 dynamic spectra, at first, we started from the frequency profiles of the radio spectrum (10 profiles per second or with time resolution of 100 ms) during the selected groups of pulses (or selected time interval). One such a profile is shown in Fig. 3a. Then for each frequency profile the wavelet spectra (WS) were calculated as shown in Fig. 3b and from this the global wavelet spectra (Fig. 4a) showing the maxima at 95% confidence level were obtained. Using this technique, we computed the distribution of significant frequency widths, in six time interval parts of the radio event (Table 1); see the histogram in Fig. 4b. Repeating the above described procedure for all time intervals of the dynamic radio spectra and considering the spectral features having 0.13 and 0.45 GHz frequency widths we constructed the filtered dynamic spectra (Figs. 5b and c).

4. Results

Using the wavelet filtering method for the August 5, 2003 event, the following spectral and temporal details of the radio spectrum were observed. As presented in Figs. 5b and c they can be divided into two components: the broadband pulses (with frequency width 0.43–0.56 GHz, average width 0.48 GHz) and the narrowband spikes (frequency width 0.08–0.18 GHz, average 0.13 GHz). During the burst intervals, the significant frequency widths remain more or less constant, though variations of individual pulses are observed.

The time evolution of the broadband pulses shows a slow negative frequency drift during the time intervals 12:45:20–12:45:50 UT and 12:47:00–12:47:15 UT (Fig. 5b) and almost linear drift during time intervals of 12:46:22–12:46:35 UT, 12:47:18–12:47:40 UT and 12:47:50–12:48:14 UT. In addition, one can see a negative drift at low frequencies during the time interval of 12:46:10–12:46:21 UT.

The filtered (0.13 GHz) radio spectra (Fig. 5c) show the presence of significant stripes of spikes in the range of 1.0–2.0 GHz. These stripes exist during all intervals of the

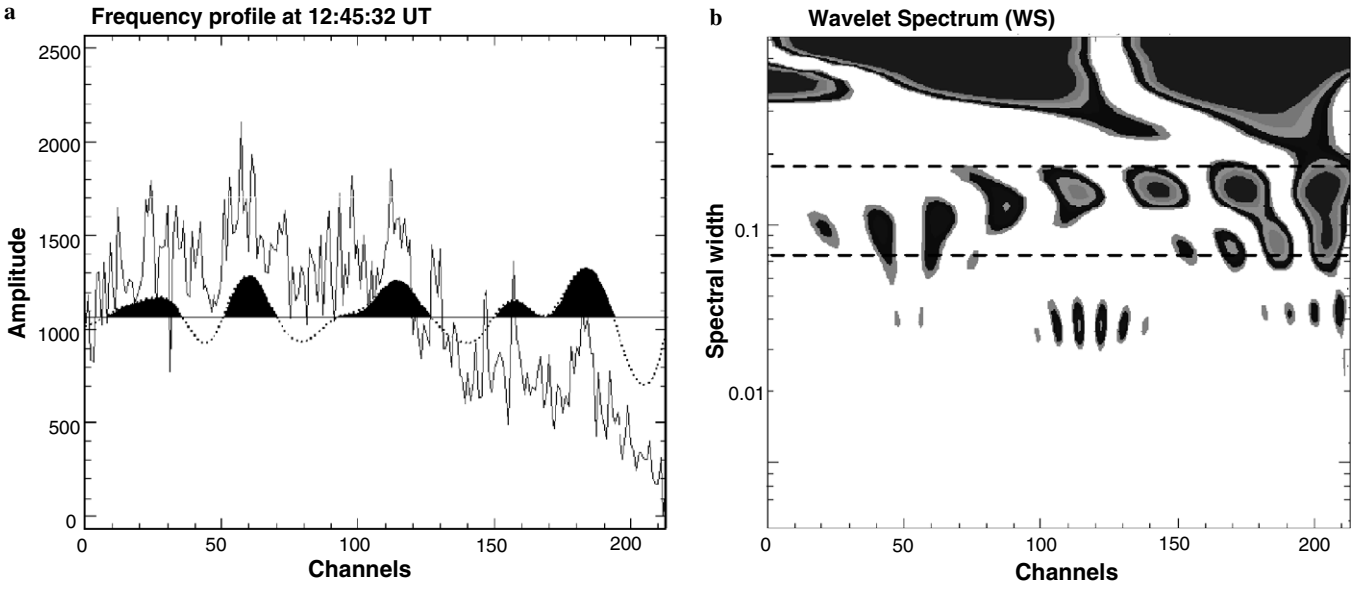

Fig. 3. (a) Frequency cut of the 1.0–2.0 GHz dynamical spectrum at 12:45:32 UT. *X*- and *Y*-axes present the frequency channels (214 channels, 1.0–2.0 GHz) and the relative radio intensity, respectively. Filled areas are cuts of spikes filtered in the frequency width of 0.08–0.18 GHz. (b) Its wavelet spectrum showing significant frequency widths: 0.43–0.56 GHz (broadband pulses) and 0.08–0.18 GHz (narrowband spikes). The intensity of the wavelet coefficients of the wavelet spectra (mother function is the Morlet function) are presented in the logarithm scale. The horizontal broken lines show the frequency region used for the spectral filtration (spikes).

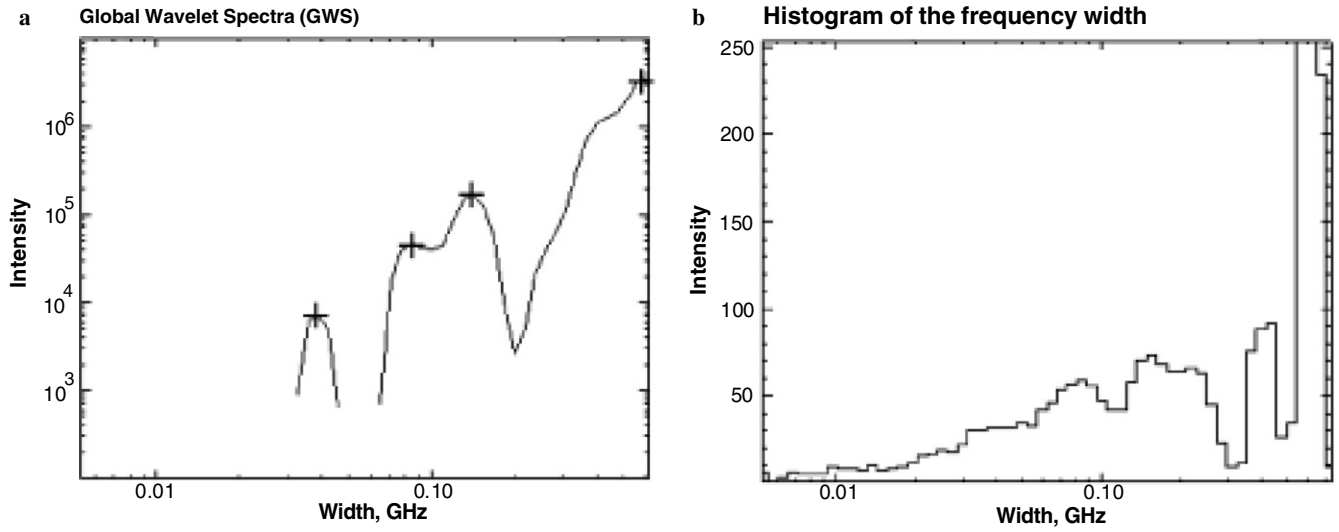

Fig. 4. (a) Global wavelet spectrum (GWS) calculated from the wavelet spectra shown in Fig. 3b in the logarithm scale. The crosses show significant frequency widths (0.04, 0.08, 0.15 and 0.56 GHz) with the 95% confidence level. (b) Summary histogram constructed for a whole time interval of the burst (12:45:25–12:48:13 UT).

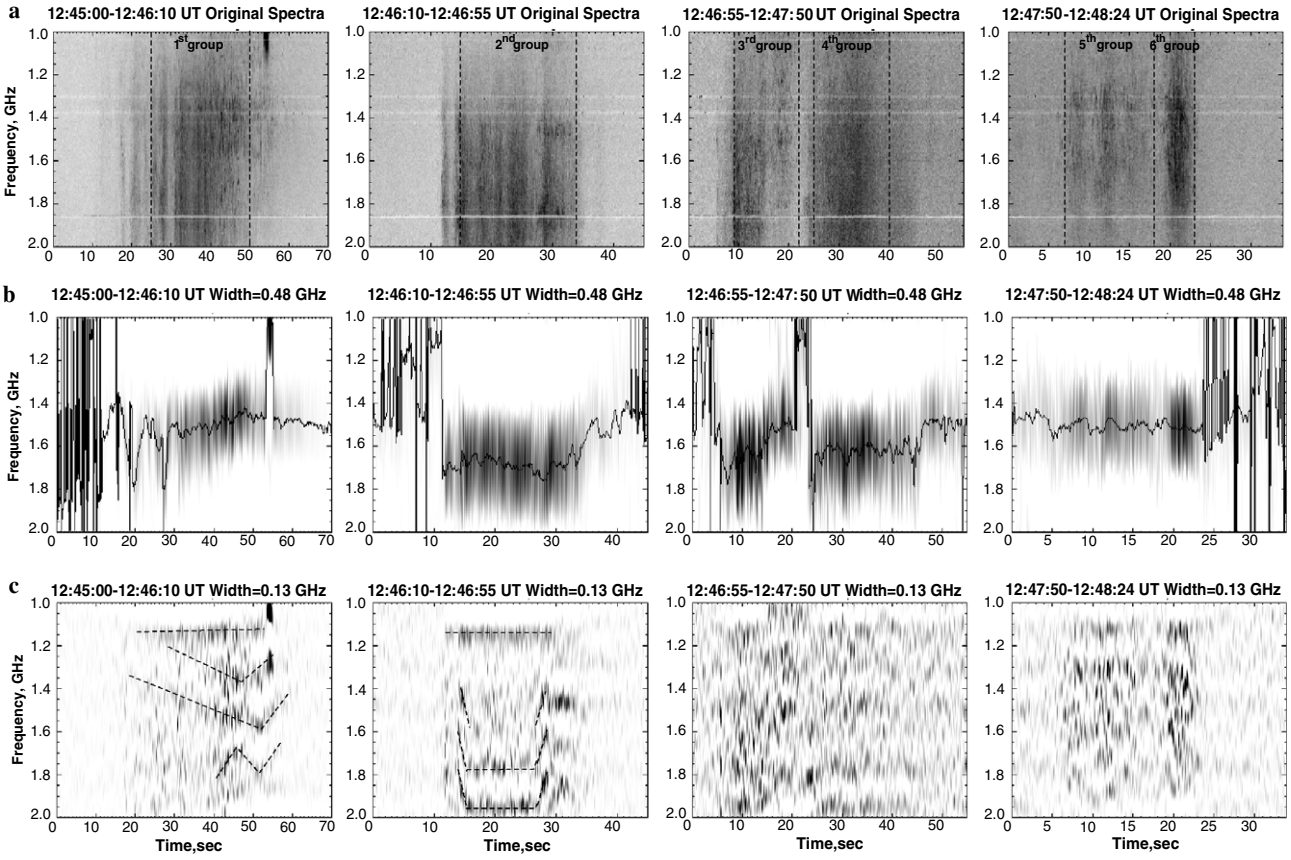

Fig. 5. (From top to bottom) The time evolution of the radio emission observed by the Ondřejov radio spectrograph with the time resolution 100 ms. The first panels (a) show the original dynamic spectrum in the 1.0–2.0 GHz range divided into four time intervals with six groups of pulses and the narrowband spikes (Table 1). The further panels – (b) and (c) show the filtered dynamic spectra for different filter frequency widths: 0.48 and 0.13 GHz. The solid line in (b) shows a time variation of the maximum intensity of the 0.48 GHz component. The broken lines in (c) show a temporal evolution of significant stripes of spikes with positive, negative drift and parallel frequency displacements.

burst, it is interesting to note a change of intensity according to the intensity of the broadband pulses. The frequencies of the stripes are ~1.15, 1.30, 1.50, and 1.75 and 1.95 GHz and the ratios of their frequencies are 1:1.1:1.3:1.5:1.7. Around 12:45:30 UT at 1.15 GHz, we recognized a splitting of one stripe into two stripes (Fig. 5c).

For the first time, it is shown (Fig. 5c, broken lines) that there are changes of frequency drift of different stripes, independently from each other, e.g., in the 12:45:20–12:46:00 UT stripe of spikes (1.15 GHz) there is no drift. However, at 1.3 and 1.5 GHz other stripes have both positive and negative drifts. In addition to this, parallel displacements of 0.2 GHz in a positive and negative sense are observed for three stripes at 12:46:24 UT and 12:46:38 UT, respectively (Fig. 5c).

To investigate the time evolution of spectral features in filtered dynamic spectra, the time profiles of these features were constructed (Figs. 6b and f) and their wavelet and global wavelet spectra were computed (Figs. 6c, d, g, and h). The broken line (Figs. 6a and e) shows the investigated part of the dynamic spectrum. It can be seen (Fig. 6g) that the narrowband spikes change period from 3 to 7 s, and from 9 to 19 s. On the other hand, for broadband pulses (Fig. 6c) we see a decrease of the significant period from 4.2 to 1.8 s.

We also analyzed the global wavelet spectrum of the time series for two stripes of the narrowband spikes at 1.15 and 1.95 GHz and for broadband pulses at 1.7 GHz. For spikes (see Fig. 6h) we found the periods 0.3–0.4 s with modulation periods of about 4.3, 9 and 16 s. Furthermore, the periods for both stripes of spikes and broadband pulses are the same. In addition, the cross-correlation analysis of the two adjacent harmonic bands reveals a peak of the correlation coefficient ($r = 0.58$) for zero time lag between profiles. Finally, using the same methods for the filtered broadband pulses and the narrowband spikes we found the time lag -0.2 s and correlation coefficient 0.72 for spikes at 1.15 GHz and the time lag 0 s and correlation coefficient 0.62 for spikes at 1.95 GHz. This result shows a peak-to-peak correlation between individual spikes in neighboring stripes of spikes and correlation between stripes of spikes with the broadband sub-second pulses.

5. Conclusions

We have developed a new method of wavelet analysis of dynamic radio spectra. This method is based on the distribution of the harmonics of global wavelet spectra for each frequency profile. From global wavelet spectra of the radio event (considering the 95% confidence level), the following significant features were recognized: (a) broadband decimetric sub-second pulses (frequency width 0.43 and 0.56 GHz, average width 0.48 GHz) and narrowband spikes (frequency width of 0.08 and 0.18 GHz, with average of 0.13 GHz). The frequency widths of these features for each group of pulses (Table 1) were almost constant in time. The narrowband spikes formed long-lived clusters (stripes). The mean frequencies of these stripes were 1.15, 1.3, 1.5, 1.75 and 1.95 GHz. On the other hand, the frequency ratios among them were ~1:1.1:1.3:1.5:1.7. At the beginning of the radio event, these ratios were varying. Furthermore, we found a frequency splitting of stripes and their slow positive frequency drift over the period of 20 s during the interval 12:45–12:46:10 UT. In the following time interval, 12:46:10–12:46:55 UT, simultaneous fast positive and negative displacements of stripes lasting about 3 s were observed. The significant period of the spikes at frequencies 1.15 and 1.75 GHz was found to be 0.38 s with modulation periods of about 4.3, 9, and 16 s. For comparison, the broadband pulses at 1.75 GHz had significant periods of 4.3, 8.2, and 16.4 s. Thus, values of some significant periods of the narrowband spikes coincide with the periods of the broadband pulses. The emission of the broadband pulses looks to be the background of the

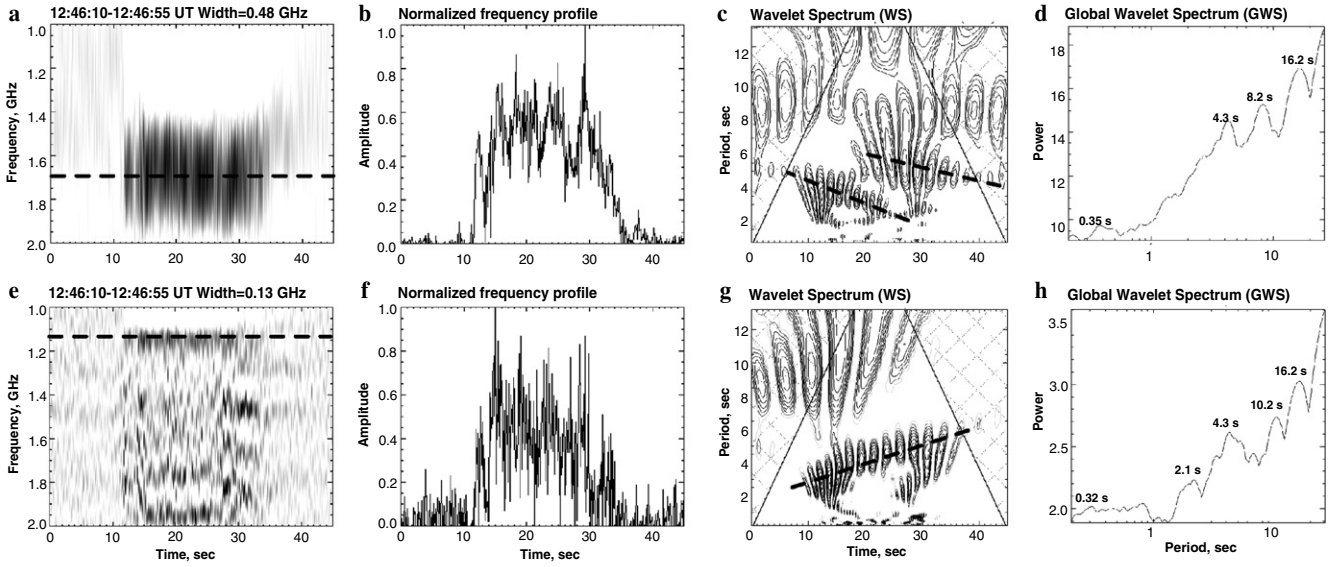

Fig. 6. The wavelet analysis of a temporal behaviour of significant frequency components. (a, e) The filtered dynamic spectra with the frequency width of 0.48 and 0.13 GHz; (b, f) the temporal profiles of the significant frequency components at 1.70 and 1.15 GHz; (c, g) present their wavelet spectra and (d, h) their global wavelet spectra. The broken lines on the wavelet spectra show drifts of the significant frequency components.

narrowband spikes. There are zero time lags between time the profiles of the broadband pulses and spikes with a significant correlation coefficient of about 0.6–0.7. These characteristics of spikes and pulses speak in favour of mutually connected sources for both these components and in favour of similar emission mechanisms. Such radio fine structures occurring over short a duration can be interpreted as a radio emission from an inhomogeneous flaring loop consisting of many thin tubes, as proposed by Koide and Sakai (1994).

Acknowledgements

Thanks are due to Prof. Barclay Clemesha for improving the quality of text of the paper. This work was supported by Russian projects of RFFR No. 03-02-16229a, 03-02-16591a, 04-02-39003a, 477.2003.2, Program RAS N30, grants NSFC 10225313, FAPESP (2003/06665-2) and A3003202 GA AS CR.

References

Astaf'eva, N.M. Wavelet analysis: basic theory and some applications. Physics-Uspekhi 39 (11), 1085–1108, 1996.

Benz, A.O. Millisecond radio spikes. Solar Physics 104, 99–110, 1986.

Benz, A.O., Güdel, M. Harmonic emission and polarization of millisecond radio spikes. Solar Physics 111 (1), 175–180, 1987.

Costa, J.E.R., Correia, E., Kaufmann, P., Brown, J.C. On removal of the gradual component in analyses of solar impulsive bursts. Astrophysical Journal Supplement Series 73, 191–197, 1990.

Donoho, D.L., Johnstone, I.M. Ideal spatial adaptation by wavelet shrinkage. Biometrika 81, 425–455, 1994.

Golyandina, N., Nekrutkin, V., Zhiglyavsky, A. Analysis of Time Series Structure SSA and Related Techniques. Charman & Hall/CRC, 2001.

Grossman, A., Morlet, J. Decomposition of Hardy functions into square integrable wavelets of constant shape. SIAM Journal on mathematical analysis 15 (4), 723–736, 1984.

Güdel, M. Solar radio spikes – Radiation at harmonics S = 2–6. Astronomy and Astrophysics 239 (1-2), L1–L4, 1990.

Huang, N.E., Shen, Z., Long, R.S. A New View of Nonlinear Water Waves – The Hilbert Spectrum. Annual Reveiw of Fluid Mechanics 31, 417–457, 1999.

Isliker, H. Structural properties of the dynamics in flare fragmentation. Solar Physics 141 (2), 325–334, 1992.

Koide, S., Sakai, J. Formation of fast magnetosonic shock waves during a two-current-loop collision in solar flares. Solar Physics 151 (1), 137–145, 1994.

Marsch, E., Tu, C.Y. Correlations between the fluctuations of pressure, density, temperature and magnetic field in the solar wind. Annales Geophysicae 11 (8), 659–677, 1993.

Meyer, Y., Roques, S., Progress in Wavelet Analysis and Applications, in: Meyer, Y., Roques, S. (Eds.), Editions Frontieres, Gif-sur-Yvette, 1993.

Milovanov, A.V., Zelenyi, L.M. Applications of fractal geometry to dynamical evolution of sunspots. Physics of Fluids B: Plasma Physics 5 (7), 2609–2615, 1993.

Torrence, C., Compo, G.P. A Practical Guide to Wavelet Analysis. Bulletin of the American Meteorological Society 79 (1), 1998.